



AMS

American Meteorological Society

Supplemental Material

[© Copyright 2019 American Meteorological Society](#)

Permission to use figures, tables, and brief excerpts from this work in scientific and educational works is hereby granted provided that the source is acknowledged. Any use of material in this work that is determined to be “fair use” under Section 107 of the U.S. Copyright Act or that satisfies the conditions specified in Section 108 of the U.S. Copyright Act (17 USC §108) does not require the AMS’s permission. Republication, systematic reproduction, posting in electronic form, such as on a website or in a searchable database, or other uses of this material, except as exempted by the above statement, requires written permission or a license from the AMS. All AMS journals and monograph publications are registered with the Copyright Clearance Center (<http://www.copyright.com>). Questions about permission to use materials for which AMS holds the copyright can also be directed to permissions@ametsoc.org. Additional details are provided in the AMS Copyright Policy statement, available on the AMS website (<http://www.ametsoc.org/CopyrightInformation>).

Supplemental Information for “Explaining scales and statistics of tropical precipitation clusters with a stochastic model”.

1. Derivation of the WTG divergence equation

We begin with the vertically-integrated budget equations temperature (T):

$$c_p \frac{\Delta p}{g} \left\langle \frac{\partial T}{\partial t} \right\rangle + \frac{\Delta p}{g} \langle \mathbf{V}_h \cdot \nabla T \rangle + \frac{\Delta p}{g} \left\langle \omega \frac{\partial S}{\partial p} \right\rangle = (L_v (P + Q_{vc}) + F_s), \quad (S1)$$

where the operator $\langle \dots \rangle$ denotes vertical averaging $\frac{1}{p_b - p_t} \int_{p_t}^{p_b} \dots dp$ between pressure levels p_b and p_t ; $\Delta p = p_b - p_t$ and g is the acceleration due to gravity. ω and \mathbf{V}_h are the vertical velocity and the horizontal velocity vector respectively. S is the dry static energy and c_p is the heat capacity of dry air. L_v is a constant that converts P and Q_{vc} from units of mm/hr to W/m^2 . ∇ is the horizontal gradient operator. We now assume that ω has the vertical structure $\Omega(p)$, such that :

$$\omega(x, y, p, t) = -\nabla \cdot \mathbf{v}_1(x, y, t) \Omega(p), \quad (S2)$$

here, $\mathbf{v}_1(x, y, t)$ captures all the horizontal and temporal variations in ω , while $\Omega(p)$ only captures the vertical structure—as in Neelin and Zeng, 2000 (NZ00). We now also invoke the WTG constraint to neglect temperature advection in (S1) to obtain:

$$c_p \frac{\Delta p}{g} \left\langle \frac{\partial T}{\partial t} \right\rangle + \nabla \cdot \mathbf{v}_1 M_s = (L_v (P + Q_{vc}) + F_s), \quad (S3)$$

where we defined a ‘gross dry stability’: $M_s = -\frac{\Delta p}{g} \left\langle \Omega \frac{\partial S}{\partial p} \right\rangle$. M_s as defined here, with $\Delta p =$

850 hPa, yields a value of $3.14 \times 10^4 \text{ kJm}^{-2}$, but it can be rescaled by dividing through by $c_p \frac{\Delta p}{g}$ to yield M_s in units of K ($\approx 3.6 \text{ K}$). Note that the use of the QTCM vertical structures (NZ00) to scale M_s results in an O(0.1) magnitude for the vertical structure associated low-level convergence $V_1(p)$ (Fig. S1).

Randomness is introduced through the temperature tendency term on the left hand side of (S3), which is split into a deterministic, domain-averaged component (indicated by the overbar) and a stochastic component:

$$\frac{\Delta p}{g} c_p \left\langle \frac{\partial T}{\partial t} \right\rangle = \frac{\Delta p}{g} c_p \left\langle \frac{\partial \bar{T}}{\partial t} \right\rangle + \xi. \quad (\text{S4})$$

We now use (S4) in (S3) to obtain:

$$\frac{\Delta p}{g} c_p \left\langle \frac{\partial \bar{T}}{\partial t} \right\rangle + \nabla \cdot \mathbf{v}_1 M_s = (L_v(P + Q_{vc}) + F_s - \xi), \quad (\text{S5})$$

which is (2) with the factor $\frac{\Delta p}{g}$ contained within the first term of (S5).

We now take the domain average of (S5), and impose the condition of domain-mean non-divergence, such that $\overline{\nabla \cdot \mathbf{v}_1} = 0$. M_s has spatial variations, due to its dependence on the amount of condensate; but for these variations are small. We can therefore assume $\overline{(\nabla \cdot \mathbf{v}_1) M_s} = 0$. We also choose our ξ such that $\overline{\xi} = 0$. The result of the domain-mean operation yields:

$$\frac{\Delta p}{g} c_p \left\langle \frac{\partial \bar{T}}{\partial t} \right\rangle = L_v(\bar{P} + \bar{Q}_{vc}) + \bar{F}_s. \quad (\text{S6})$$

Subtracting (S6) from (S5) leads to (3).

The water vapor (q_v) and the condensate (q_{cond}) are also similarly truncated with structure functions $b_{vap}(p)$ and $b_{cond}(p)$ respectively. All the vertical structure functions are indicated in Fig. S1. Note that q_{cond} is the layer average over the depth Δp of the troposphere, even though the condensate is only assumed to occupy the upper troposphere ($p < 400$ hPa) with a vertically invariant structure function b_{cond} . Similar to M_s , we have definitions for M_{qp} and M_{qpc} :

$$M_{qp} = \frac{-1}{\langle b_{vap} \rangle} \left\langle \frac{\partial \Omega}{\partial p} b_{vap} \right\rangle \quad (\text{S7})$$

$$M_{qpc} = -\frac{1}{\langle b_{cond} \rangle} \left\langle \frac{\partial \Omega}{\partial p} b_{cond} \right\rangle. \quad (\text{S8})$$

2. Construction and analysis of the rotational wind field

Stochastic fields with spatial correlations are used to generate the rotational wind field. A white stochastic vorticity field is generated in a similar manner to stochastic flux convergence using σ_{vort} and τ_{vort} in lieu of σ and τ_{noise} respectively, in (6) of the main article. The only difference is that this white stochastic vorticity field has a characteristic time scale (τ_{vort}) of 12 hours, reflecting the persistent nature of the vorticity field. This white-in-space vorticity is transformed into a red-in-space vorticity field by manipulating its spectral coefficients; we first take the Fourier transform of the white vorticity field and then multiply its Fourier components by $\frac{k_0}{k_x^2 + k_y^2 + k_0^2}$. Here k_x and k_y are the horizontal wavenumbers and k_0 is the decorrelation wavenumber. A subsequent inverse Fourier transform ensures that the resulting vorticity field is red in space. For the red vorticity field, k_0 is chosen to be 1, such that the decorrelation scale of the vorticity field is \sim wavenumber 1. The red vorticity field is inverted using the Poisson solver with Dirichlet boundary conditions to ensure that \vec{v}_{rot} is zero across the northern and southern boundaries.

Fig. S3 shows a snapshot of the rotational wind field at the same time as the sample precipitation field shown in Fig. 1. The large-scale nature of the rotational wind is apparent with the vortex in the north-eastern corner of the domain. Fig. S4 shows the probability distribution functions of the rotational wind velocities averaged over the lower troposphere, from 100 days of the model run. The u and v velocities have rms velocity values close to 5 m/s.

3. Sensitivity to the condensate amount

In our standard case, cloud condensate (i.e., condensate in a size range small enough to rain out slowly and be significantly transported, governed by equation (5)) production only begins at saturation, which produces very little condensate rain. We can increase the fraction of condensate rain, relative to strong convective rain by changing the threshold value of condensate production (q_{vc}). We display our sensitivity results in Figs. S5 and S6 for three cases: no condensate, $q_{vc} = 67.5$ mm and $q_{vc} = 65$ mm. Note that there is greater condensate production in the latter than in the former. Fig. S5 shows the snapshot on the same day as Fig.1. Also note that our noise is generated from the same pseudorandom generator, so the stochastic fields are identical in all the runs. Fig. S5 shows quantitative changes to the precipitation intensity when the condensate production rates are increased, but the qualitative nature of the precipitation clustering is unchanged. Fig. S6 shows the cluster pdfs for the same three cases. The slopes of the pdfs are not changed by differences in the condensate production amounts, but there are quantitative changes to the cutoffs. Both the cluster area

and power cutoffs reduce upon condensate production, but the changes to cluster area cutoff is smaller than the change to the cluster power cutoff. Overall, the effect of increased condensate in these experiments is to reduce the cluster rain intensity, because the range of high q_v with intense convective rain is reduced as q_{vc} is reduced. The rain associated with cloud condensate is commonly not large enough to meet the threshold to be included in the cluster diagnostics. More sophisticated parameterization of cloud processes, or consideration of clusters based on other criteria would affect this quantitatively. Overall, the results here are reasonably robust to the inclusion of condensate production, which mainly enters for parameters that tend to give excursions into the very high moisture range.

4. Probability distribution of the branching process

The derivation that leads to the form (16) is fairly well-known in the branching process literature and is reconstructed here with borrowed elements from Hawkins and Ulam (1944), Good (1949) and Wendel (1967). A branching process with identical and independent branching probability across generations is first considered. For analogies with precipitation clusters, certain precipitating pixels are identified as seeds, and pixels that subsequently emerge adjacent to this seed are termed branches. The first part of the derivation concerns the relationship between the branching probability and the probability distribution of the tree (or cloud cluster) size. A specific form for the branching probability—the Poisson distribution—is inserted into this expression, with suitable approximations to obtain (16). The robustness of (16) to small number of mergers between trees is also noted.

Branches that arise within a specified time interval are assumed to belong to the same generation. $p_1^{(r)}(m)$ is the probability of spawning m branches from r initial seeds in one generation, where m and r are non-negative integers. $q_k(s)$ is the probability that the *total number of branches* after k generations is s ; for our purposes, this is the probability distribution of the cluster size. For a branching process that commences from a single seed the following expression can be written for $q_k(s)$ (Good 1949):

$$q_k(s) = \sum_{C_s} p_1^{(1)}(m_1) p_1^{(m_1)}(m_2) p_1^{(m_2)}(m_3) \dots p_1^{(m_{k-2})}(m_{k-1}) p_1^{(m_{k-1})}(m_k) . \quad (S9)$$

Fig. A4 provides a visual representation of the variables r , k , m_k and s . (S9) assumes that the branching process is Markovian: the number of branches in each generation is solely dependent on the number of seeds in the preceding generations. C_s refers to all combinations that satisfy the constraint $1 + m_1 + m_2 + \dots + m_{k-1} + m_k = s$.

$q_k(s)$ is the target probability distribution that must be solved for in terms of $p_1^{(1)}(m)$. The concept of probability generating functions (pgfs) for discrete probability functions is useful in

this regard. If X and Y are random variables (rvs) with discrete probability distribution functions, $p_1^{(r)}$ and q_k respectively, then their pgfs are defined by:

$$f_X(z) = \sum_{t=0}^{\infty} p_1^{(1)}(X=t)z^t \quad (\text{S10})$$

$$g_{Y,k}(z) = \sum_{t=0}^{\infty} q_k(Y=t)z^t. \quad (\text{S11})$$

In (S10), X denotes the number of branches that arise in each generation from a single seed. In (S11), Y denotes the total number of branches in the tree after k generations. A property of pgfs that will feature repeatedly in this derivation is that for independent rvs, the pgf of the sum of the rvs is the product of the pgfs. For example, if $X = X_1 + X_2 + X_3 + \dots + X_j$, then

$$f_X(z) = f_{X_1}(z)f_{X_2}(z)\dots f_{X_j}(z). \text{ If } X_1, X_2 \dots X_j \text{ are identical, then } f_X(z) = [f_{X_1}(z)]^j.$$

(S9) and (S11) are combined to obtain an expression for $g_Y(z)$:

$$g_{Y,k}(z) = \sum_{t=0}^{\infty} \left(\sum_{C_t} p_1^{(1)}(m_1) p_1^{(m_1)}(m_2) p_1^{(m_2)}(m_3) \dots p_1^{(m_{k-2})}(m_{k-1}) p_1^{(m_{k-1})}(m_k) \right) z^t. \quad (\text{S12})$$

C_t is the number of combinations of non-negative integer values of $m_1, m_2 \dots m_k$ satisfying the constraint $1 + m_1 + m_2 + \dots + m_k = t$.

A fair amount of algebra and Good (1949) confirm that (S12) can be rewritten as:

$$g_{Y,k}(z) = \sum_{t'=0}^{\infty} \left(\sum_{C_{t'}} p_1^{(1)}(m_1) p_1^{(m_1)}(m_2) p_1^{(m_2)}(m_3) \dots p_1^{(m_{k-2})}(m_{k-1}) z^{t'} z \sum_{t=0}^{\infty} p_1^{(m_{k-1})}(t) z^t \right), \quad (\text{S13})$$

where the terms involving $p_1^{(m_{k-1})}(m_k)$ from (S12) have been factored out, and $C_{t'}$ is the combination such that $m_1 + m_2 + \dots + m_{k-1} = t'$.

Now, $\sum_{t=0}^{\infty} p_1^{(m_{k-1})}(t)z^t = [f_X(z)]^{m_{k-1}}$ from the definition of the pgf in (S10) and the property linking the pgfs of independent identically distributed sums of rvs. This reduction procedure is repeated and is used to factor out successive terms involving $p_1^{(m_{k-2})}(m_{k-1})$, $p_1^{(m_{k-3})}(m_{k-2})$ etc. The result is the iterated expression:

$$g_{Y,k}(z) = z f_X \left(\underbrace{z f_X(z)}_{k-3 \text{ times}} \right) \quad (\text{S14})$$

or the following implicit equation:

$$g_{Y,k} = zf_X(g_{Y,k-1}).$$

For unchanging total number of branches in successive generations $g_{Y,k} \approx g_{Y,k-1}$. Upon dropping the subscripts indicating the rvs, the following concise expression for $g(z)$ is obtained (Hawkins and Ullam 1944, Good 1949):

$$g(z) = zf[g(z)]. \quad (S15)$$

The target expression $q_k(s)$ is contained with the pgf, $g(z)$. $q_k(s)$ as defined in (S9) is the probability that the total number of branches after k generations is of size s , when *starting from a seed of size 1*. $p_1^{(r)}$ is the pdf of a rv composed of a sum of r rvs, each with the identical pdf $p_1^{(1)}$. In other words, r different seeds branch out independently of each other.

When starting out with a seed of size r the corresponding pgf for $p_1^{(r)}$ will be $(g(z))^r$, with the associated implicit function:

$$(g(z))^r = zf[(g(z))^r]. \quad (S16)$$

Lagrange's inversion theorem for complex analytic functions (Wendel 1967) is used to solve(S16), with the following power series solution for $(g(z))^r$:

$$(g(z))^r = \sum_{s=1}^{\infty} \frac{z^s}{s!} \left[\frac{d^{s-1}}{dt^{s-1}} (rt^{r-1} f(t)^s) \right]_{t=0}. \quad (S17)$$

Since pgfs are complex analytic functions by definition, the property relating the pgfs of independent rvs is used to rewrite (S17):

$$g(rz) = \sum_{s=1}^{\infty} \frac{z^s}{s!} \left[\frac{d^{s-1}}{dt^{s-1}} (rt^{r-1} f(st)) \right]_{t=0}. \quad (S18)$$

Expanding (S18) leads to:

$$g(rz) = \frac{r}{s} p_1^{(s)}(s-r) z^s. \quad (S19)$$

$g(rz)$ is expanded as $\sum_{s=0}^{\infty} q^{(r)}(s) z^s$ and then matched with the coefficients of z^s to get:

$$q^{(r)}(s) = \frac{r}{n} p_1^{(s)}(s-r). \quad (S20)$$

The probability distribution of the size of the tree is now related to the branching probability itself. Up until now, the branching probability $p_1^{(1)}(m)$ remained unspecified. We now assume the Poisson distribution for $p_1^{(1)}(m)$, with the parameter:

$$p_1^{(1)}(X = w, \lambda) = \frac{e^{-\lambda} \lambda^w}{w!}, \quad (\text{S21})$$

which is the probability that the Poisson distributed rv $X = w$. λ is the average number of branches in a single generation. The Poisson distribution of the sum of s independent and identical distributions leads to another Poisson distribution with the parameter $s\lambda$. Therefore

$p_1^{(s)}(X = w, \lambda) = \frac{e^{-s\lambda} (s\lambda)^w}{w!}$. This expression is plugged into (S20), to finally obtain:

$$q^{(r)}(s) = \frac{r e^{-s\lambda} (s\lambda)^{(s-r)}}{s (s-r)!}. \quad (\text{S22})$$

Stirling's approximation, $s! \approx \sqrt{2\pi s} \left(\frac{s}{e}\right)^s$ is used in place of the factorial in the denominator of (S22):

$$q^{(r)}(s) = \frac{1}{\sqrt{2\pi}} \frac{r}{\lambda^r} \frac{1}{s^{\frac{3}{2}}} \frac{e^{-s(\lambda - \ln \lambda)}}{e^r} \left(1 - \frac{r}{s}\right)^{-\left(s-r+\frac{1}{2}\right)}. \quad (\text{S23})$$

Stirling's approximation is acceptable even for small integer values (error is ~4% for $s = 2$, and monotonically reduces with increases in s).

For small r and large s , $\left(1 - \frac{r}{s}\right)^{-\left(s-r+\frac{1}{2}\right)} \approx e^r$, leading to:

$$q^{(r)}(s) = C(\lambda, r) s^{\frac{3}{2}} e^{-\frac{s}{s_L}}. \quad (\text{S24})$$

Where $s_L = 1 - \lambda - \ln \lambda$ and $C(\lambda, r)$ is a parameter that depends on the mean number of branches λ and the number of initial seeds r . The cluster size generated from r initial seeds is equivalent to cluster size generated by mergers between r clusters, each of which is generated from a single seed.

For the special case of $r = 1$ in (S22):

$$q(s) = \frac{e^{-s\lambda} (s\lambda)^{(s-1)}}{s!}. \quad (\text{S25})$$

(S25) can also be reduced using Stirling's approximation to yield $q(s) = C(\lambda)s^{-\frac{3}{2}}e^{-\frac{s}{s_L}}$. Note that the pdfs described by (S25) and (S22) have special names: the Borel distribution and the Borel-Tanner distribution respectively.

In conclusion, the probability distribution of the total size of a tree generated by the branching process with a Poisson branching probability, $P(x) \sim x^{-1.5}e^{-\frac{x}{x_L}}$ and the form of the distribution is robust to a small number of mergers between trees. Note that one could also substitute alternate forms of $p_1^{(1)}(s-r)$ in (S22) to test the effects of other functional forms for the branching probability.

5. Exotic parameter regimes

To highlight clusters driven by radiative instabilities in the non-stochastic model, we configured to run our model with diminished values of stochastic forcing (by a factor of 500) and surface evaporation (by a factor of 10). ϵ_R and ϵ_{cloud} in **(14)** and **(15)** now have values of 5 W/m² per mm of CWV and 5 W/m² per mm/h of precipitation respectively. To create homogeneous conditions, the mock Hadley cell was not imposed, and the impact of rotational wind advection is tested in one of the runs. Note that this model version without stochastic forcing is close to the coarsening model of Craig and Mack (2013).

Four different model runs are shown in Fig. S9, three of which highlight the different aggregated features that can emerge under such quiescent conditions. The snapshots shown in Figs. S9a,b and d are at statistically steady-state: marked by unchanging cluster characteristics (and also only small variations in the visual appearance). Fig. S9a is a snapshot of the CWV field from the quiescent model simulation, in the presence of rotational wind advection. With reduced stochastic forcing in the divergence, CWV does not vary much beyond $q_c = 60$ mm and shows no inclination to aggregate. Fig. S9b shows how the removal of rotational advection causes the model CWV field to aggregate into a column. Fig. S9c is a snapshot of the model run without diffusion or rotational advection that produces long, thin regions of enhanced CWV regions surrounded by dry regions. The CWV features in this run did not attain steady-state and continued to gradually change even when run up to 400 days (although the qualitative appearance remained the same). The aggregated features in Fig. S9c are reminiscent of the cellular appearance of some marine stratocumulus clouds (Stevens et al. 2005; Wang and Feingold 2009). There is also some resemblance to the wispy CWV features presented in the global RCE simulations of Reed and Chavas 2015 (see their Fig.1, 'ne120' configuration). When the model is initialized with an aggregated Gaussian blob but run without any form of advection, the CWV stays aggregated, as shown in Fig. S9d.

Figures

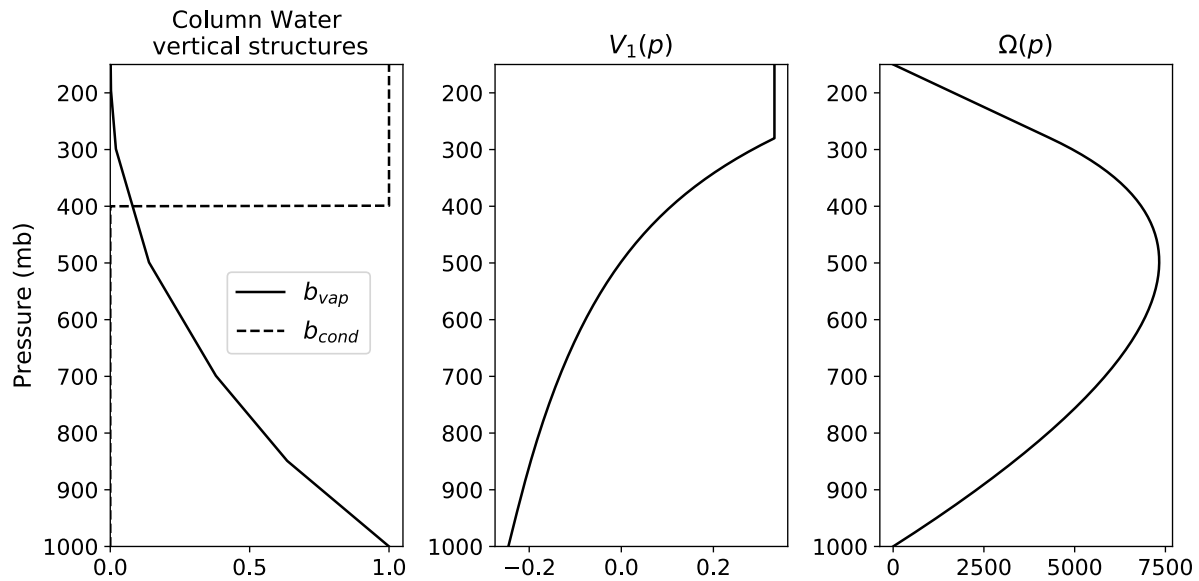


Figure S1. The vertical structures for the water vapor (b_{vap}), condensate (b_{cond}), the horizontal wind (V_1) and the vertical velocity (Ω) used in model derivation.

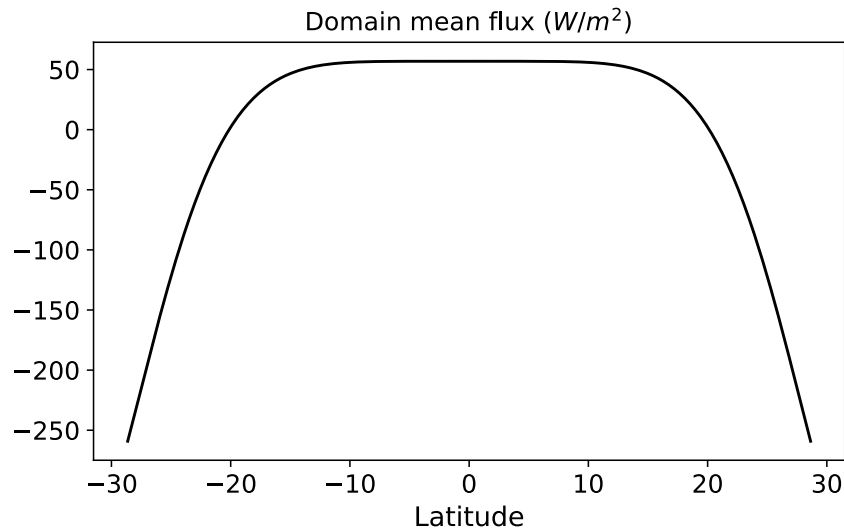


Figure S2. The externally imposed latitudinally varying domain mean flux mimicking a Hadley Cell. This structure produces a divergence field that results in upper-level divergence in the middle of the domain and upper-level convergence near the northern and southern boundaries.

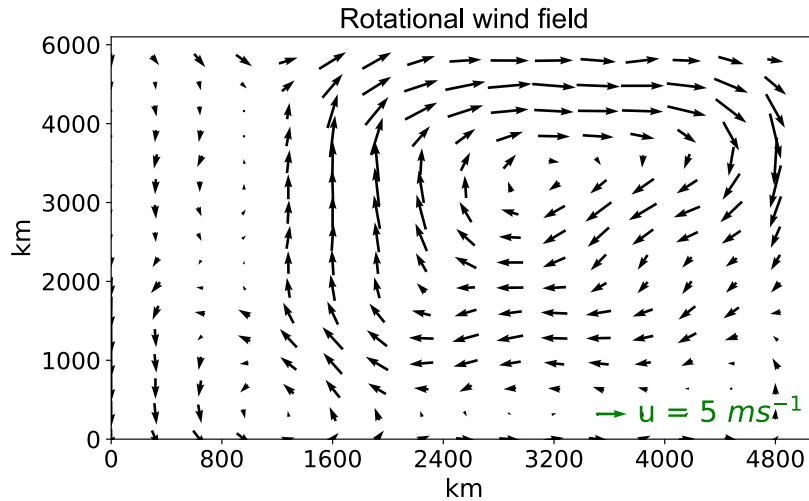


Figure S3. A snapshot of the rotational wind vector at the same instant as **Figure 1** in the article.

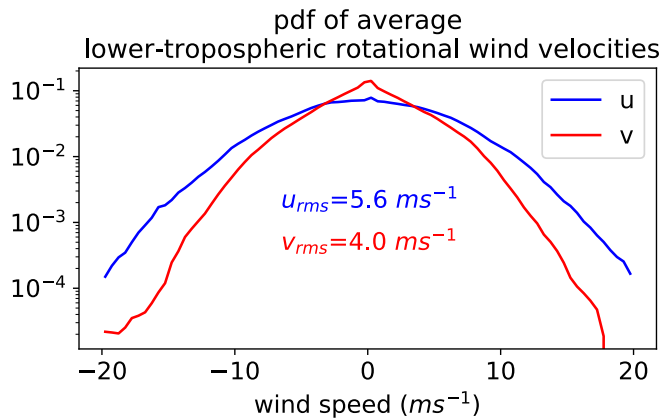


Figure S4. The probability distributions of the rotational wind velocities averaged over the lower troposphere for the x (blue) and y (red) directions, along with the root mean square values of the rotational wind velocities.

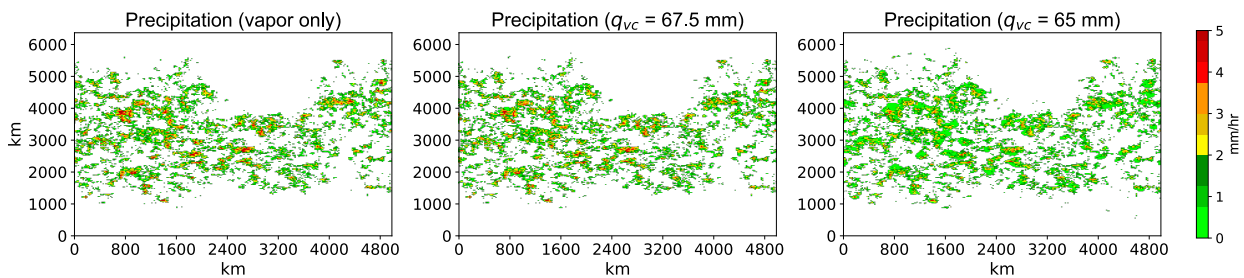


Figure S5. Snapshots of the precipitation field at the same instant as **Figure 1** in the main text for three runs with different amounts of condensate production (No condensate, weak condensate and strong condensate production). Note that the same set of pseudorandom numbers are used in each run, ensuring ease of comparison.

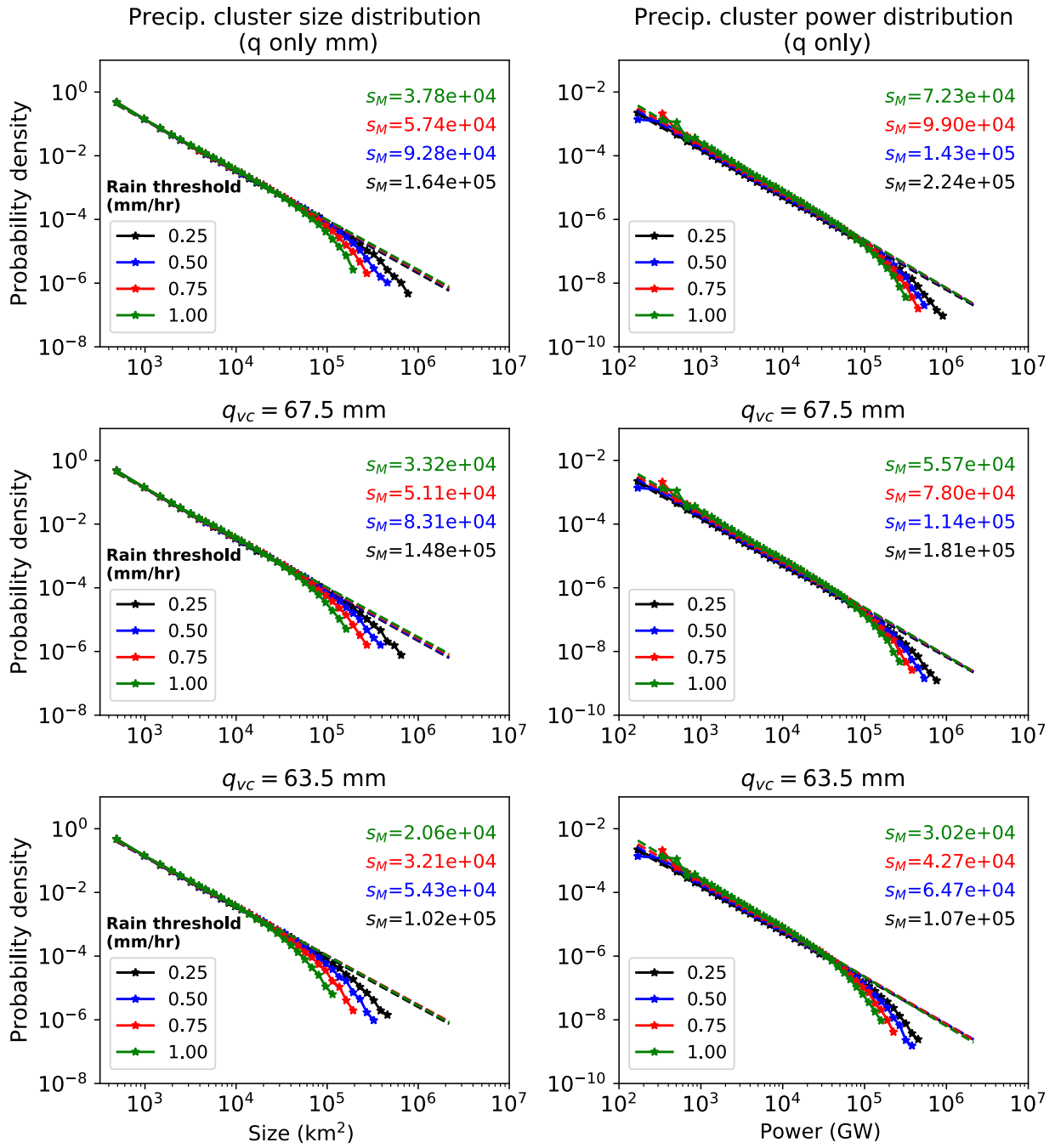


Figure S6. The cluster pdfs of the cluster area (left column) and cluster power (right column) for three different cases of condensate production. Row 1: no condensate production, Row 2: moderate condensate production and Row 3: strong condensate production.

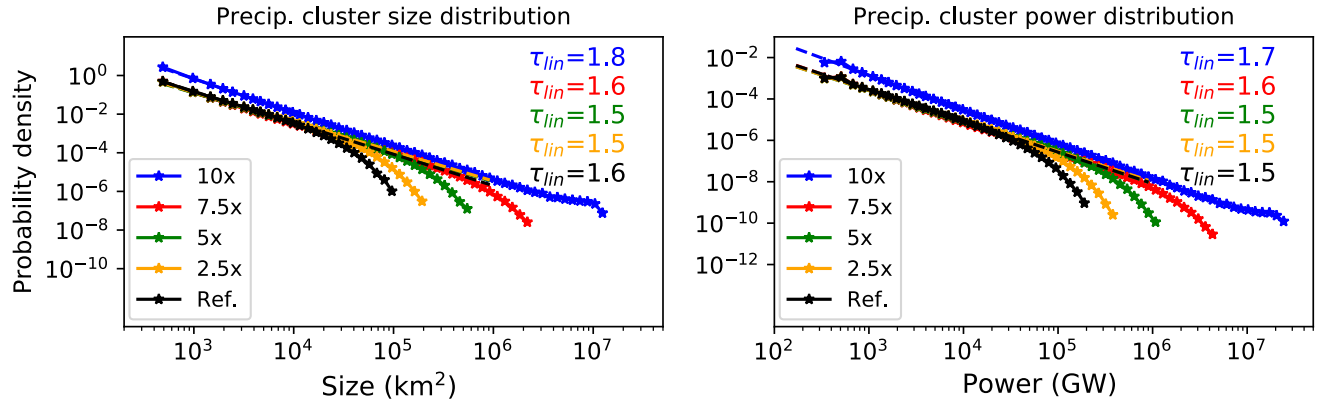
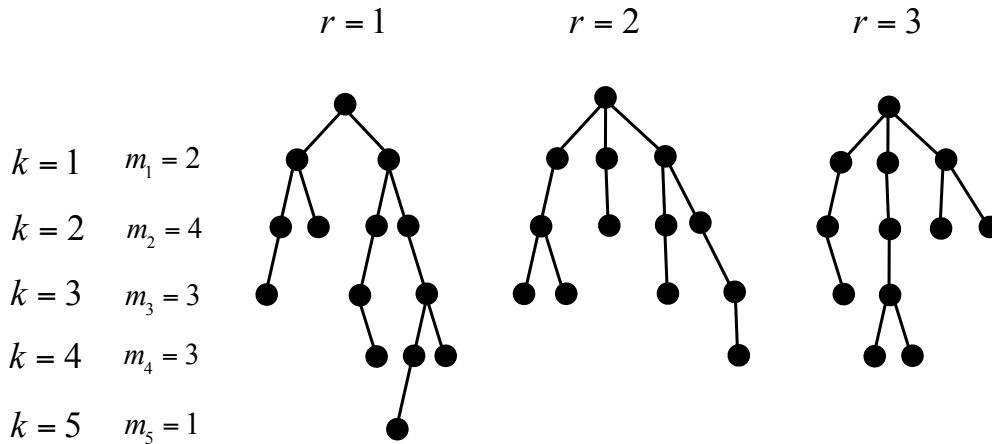


Figure S7. The cluster pdfs (for 1 mm/h threshold) as a function of increasing evaporation rate. The standard case ($E = .14$ mm/h) is in black. The other curves are multiples of the reference case evaporation rate. The slopes are computed using a linear regression over the power-law portion of the curve. Note how the slope increases as the cutoff x_L gets closer to the domain size (percolation). Beyond percolation, a long scale-free range and a bump corresponding to the domain size is seen (blue).



$$1 + m_1 + m_2 + m_3 + m_4 + m_5 = s_1 = 14$$

Figure S8. A visual depiction of the variables that appear in the derivation of the stochastic branching process. The branching process can commence from r initial seeds and proceed across k generations. At each generation, there are m_k number of branches. The total number of branches across all generations, $s = 1 + \sum_k m_k$. The evolution of the branching process up $k = 5$ generations is depicted. Note that the probability of branching from a single seed is governed by the same pdf, $p_1^{(1)}$, across all generations.

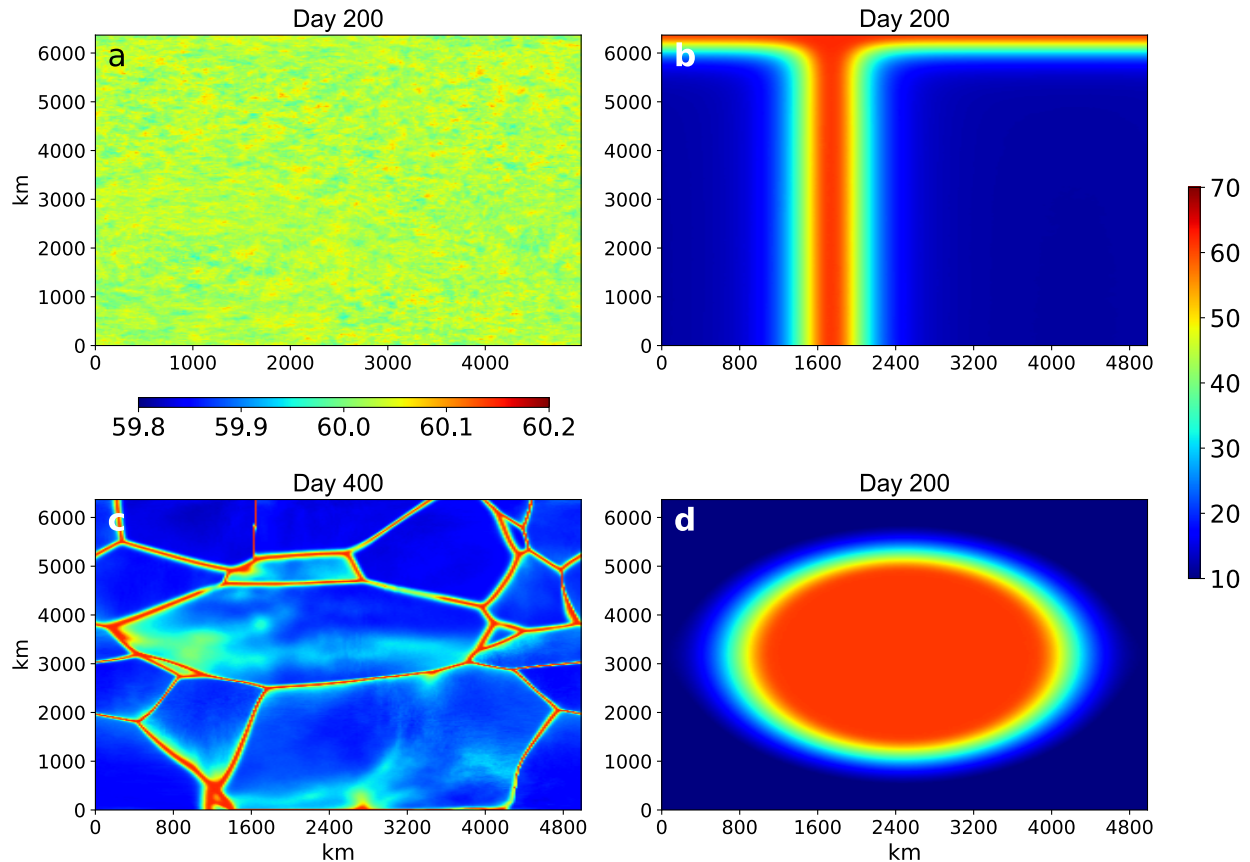


Figure S9. Examples of radiatively driven self-aggregated regions of CWV in four different runs with near-zero stochastic forcing (σ reduced by a factor of 500 from its reference value). These runs were also conducted with reduced E (by a factor of 10). The radiative effects of CWV and clouds were also modified ($\epsilon_r = 5 \text{ Wm}^{-2}\text{mm}^{-1}$, $\epsilon_{cloud} = 5 \text{ Wm}^{-2}\text{mm}^{-1}\text{hr}$). a) model run including rotational wind. b) same run as a) but without rotational wind. c) same as a) but without rotational wind and diffusion. d) same as a) but without rotational wind and advection, and starting from aggregated initial condition. The vertical color bar on the right is for CWV values (in mm) in panels b), c) and d). The horizontal color bar—with a narrow range—indicates CWV values (in mm) in panel a).

References

- Craig, G. C., and Mack, J. M. (2013), A coarsening model for self-organization of tropical convection, *J. Geophys. Res. Atmos.*, 118, 8761– 8769, doi:[10.1002/jgrd.50674](https://doi.org/10.1002/jgrd.50674).
- Good, I. J., 1949: The number of individuals in a cascade process. *Proceedings of the Cambridge Philosophical Society*, 45, 360-363.
- Hawkins, D. and S.M Ulam, 1944: Theory of Multiplicative Processes: Technical Report LA-171, Los Alamos Scientific Laboratory.
- Reed, K. A., and Chavas, D. R. (2015), Uniformly rotating global radiative-convective equilibrium in the Community Atmosphere Model, version 5, *J. Adv. Model. Earth Syst.*, 7, 1938– 1955, doi:[10.1002/2015MS000519](https://doi.org/10.1002/2015MS000519).
- Neelin, J. D., and N. Zeng, 2000: A quasi-equilibrium tropical circulation model - Formulation. *Journal of the Atmospheric Sciences*, 57, 1741-1766.
- Wendel, J. G. (1975): Left-Continuous Random Walk and the Lagrange Expansion. *The American Mathematical Monthly*, 82(5), 494-499. doi:10.2307/2319745